

Mechanism of Xylobiose Hydrolysis by GH43 β -Xylosidase

Ian J. Barker, Luis Petersen, and Peter J. Reilly*

Department of Chemical and Biological Engineering, Iowa State University, Ames, Iowa 50011, United States

Received: August 19, 2010; Revised Manuscript Received: September 25, 2010

Glycoside hydrolases cleave the glycosidic linkage between two carbohydrate moieties. They are among the most efficient enzymes currently known. β -Xylosidases from glycoside hydrolase family 43 hydrolyze the nonreducing ends of xylooligomers using an inverting mechanism. Although the general mechanism and catalytic amino acid residues of β -xylosidases are known, the nature of the reaction's transition state and the conformations adopted by the glycon xylopyranosyl ring along the reaction pathway are still elusive. In this work, the xylobiose hydrolysis reaction catalyzed by XynB3, a β -xylosidase produced by *Geobacillus stearothermophilus* T-6, was explicitly modeled using first-principles quantum mechanics/molecular mechanics Car–Parrinello metadynamics. We present the reaction's free energy surface and its previously undetermined reaction pathway. The simulations also show that the glycon xylopyranosyl ring proceeds through a $^{2,5}\text{B}$ -type transition state with significant oxacarbenium ion character.

1. Introduction

Glycoside hydrolases (GHs) catalyze hydrolysis of the glycosidic bond between two carbohydrate residues or between a carbohydrate and a noncarbohydrate moiety. Spontaneous hydrolysis of this linkage has an estimated half-life of over 5 million years.¹ GHs may accelerate this reaction by 10^{17} times the spontaneous rate, placing them among the most efficient catalysts studied. In general, GH active sites are highly specific for substrate binding and catalyze hydrolysis using a general acid and a general base.² The spatial arrangement of these residues in each enzyme active site determines whether the product anomeric configuration is inverted or retained during hydrolysis.

The CAZy (Carbohydrate-Active enZYme) database classifies GHs and other carbohydrate-active enzymes into families by amino acid sequence, implying that all family members share a common ancestry and mechanism and a similar overall protein fold.³ Of the 100+ GH families found in CAZy, GH family 43 (GH43) members, many of which are β -xylosidases (EC 3.2.1.37), come almost exclusively from bacteria, fungi, and plants. *Geobacillus stearothermophilus* T-6 specifically produces XynB3, an inverting GH43 β -xylosidase with β -sandwich and five-bladed β -propeller domains (Figure 1).⁴ Its active site is a pocket, closed off at one end by a single loop at the end of the β -sandwich domain that binds one xylosyl residue at a time. The enzyme exhibits exo action, releasing single xylosyl units from the nonreducing ends of short xylooligomers.⁵

Inverting GHs use a single-displacement mechanism in which one carboxylic acid acts as a general base/nucleophile and another acts as a general acid/proton donor, involving an oxacarbenium ion transition state (TS).⁶ In XynB3, Asp15 and Glu187 are the general base and general acid, respectively (Figure 2).⁵ Asp15 coordinates a water molecule that attacks the glycon C1' atom, and Glu187 protonates the leaving group at the glycosidic oxygen atom.

Recently obtained XynB3 crystal structures of E187G and D128G mutants have xylobiose molecules in the active site.⁴

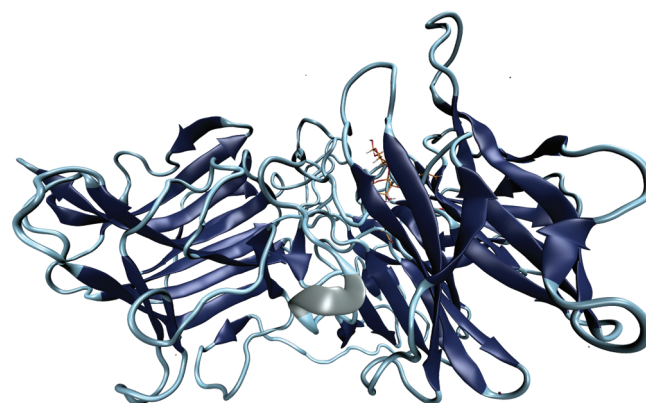


Figure 1. Structure of XynB3 showing its β -sandwich domain (left) and five-bladed β -propeller domain (right) that form a pocket-shaped active site.

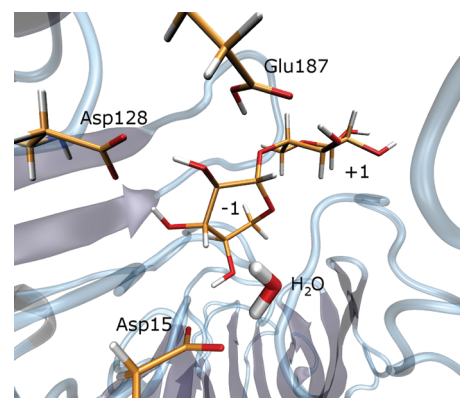


Figure 2. A view of the XynB3 active site with bound β -xylobiose, general base Asp15 coordinating the catalytic water molecule, and general acid Glu187.

Each crystal structure is a tetrameric complex of XynB3 enzymes, all binding xylobiose molecules. Interestingly, the xylosyl rings bound to subsite -1 have different conformations, even for the same mutant. In the proton donor mutant (E187G), two xylosyl rings are in a $^4\text{C}_1$ chair (the most stable conformation

* Corresponding author. Telephone: +1-515-294-5968. Fax: +1-515-294-2689. E-mail: reilly@iastate.edu.

in solution) and the other two are in a mixed $^2\text{S}_0/{}^{2,5}\text{B}$ conformation. The D128G mutant has one xylobiose molecule in a ${}^4\text{C}_1$, two in a $^2\text{S}_0/{}^{2,5}\text{B}$, and one in an ${}^0\text{E}$. Glycon ring distortion of the Michaelis complex away from the ${}^4\text{C}_1$ conformation is a common feature of β -glycosidases.^{7–10}

In this work, we model the hydrolysis of the β -1,4 glycosidic bond in xylobiose by GH43 β -xylosidase using first-principles quantum mechanics/molecular mechanics (QM/MM) Car–Parrinello metadynamics to obtain insight into the detailed mechanism of the enzyme. In addition, we provide new structural and dynamical information for the wild-type Michaelis complex, TS, and product states. Furthermore, we followed the conformational itinerary of the glycon xylosyl ring along the hydrolysis reaction.

2. Computational Methods

Most of the computational methods are very similar to those presented elsewhere.^{11,12} Therefore, we focus on the important details that are specific for this simulation.

2.1. Classical Molecular Dynamics and System Setup. XynB3 GH43 β -xylosidase (Protein Data Bank structure 2EXJ) was subjected to classical molecular dynamics (MD) using the Amber9¹³ software package. This was done to obtain a fully solvated structure, equilibrated at natural conditions. The FF99SB¹⁴ Amber force field was used to model the protein, and the GLYCAM06¹⁵ force field was used to model the xylobiose substrate. The D128G mutation was corrected manually to simulate the wild-type active site using PyMOL (<http://www.pymol.org/>). Glu187 was protonated, and Asp15 was unprotonated on the basis of prior knowledge of the inverting reaction mechanism. The protonated states of ionizable amino acids were selected on the basis of their microenvironment. The remaining aspartate and glutamate residues were modeled in their unprotonated state, while His151, His210, His253, and His362 were protonated to a charge of +1. The other seven histidine residues were simulated in their neutral states. The original crystal-structure water molecules were retained, and a water box of 10 Å from the protein surface was added and modeled using the TIP3P force field.¹⁶ Eleven sodium ions were added to neutralize the system. The simulation was stopped after 2 ps, when the structure was equilibrated. The equilibrated structure was used as a starting point for the QM/MM calculation, from which substrate-enzyme binding and reaction details can be obtained.

2.2. QM/MM Molecular Dynamics. The QM/MM implementation of Laio et al. within the Car–Parrinello MD scheme was used.^{17,18} The QM region was defined as a $14.9 \times 18.1 \times 19.5$ Å box containing 55 atoms and including the side chains of Asp15 (capped at the β -carbon atom) and Glu187 (capped at the γ -carbon atom). The nucleophilic water molecule was also included in this region. Kohn–Sham orbitals were expanded in a plane-wave basis set with an 80-Ry kinetic energy cutoff. Ab initio pseudopotentials were generated by the Troullier–Martins scheme.¹⁹ The Perdew–Burke–Ernzerhoff functional²⁰ was used in the generalized gradient-corrected approximation of density functional theory on the basis of its reliability in describing hydrogen bonds.²¹

The structure was optimized using QM/MM MD by annealing the electronic velocities until the maximal component of the nuclear gradient was 10^{-4} au. The annealing simulation time step was 0.072 fs, and the fictitious electron mass was 1000 au. The MD simulation coupled to a thermostat had a time step of 0.12 fs and a fictitious electron mass of 700 au.

2.3. QM/MM Metadynamics. For this system, a difference of coordination numbers (CN) was used as collective variables

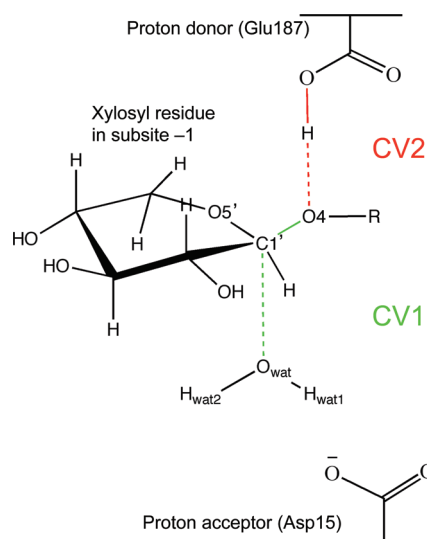


Figure 3. Collective variables (CV1 in green and CV2 in red) used to model hydrolysis of the xylobiose glycosidic bond.

(CV). Two CVs were used to indicate reaction progress (Figure 3). CV1 is $\text{CN}_{\text{C}1',\text{O}4} - \text{CN}_{\text{C}1',\text{O}_{\text{wat}}}$, a measure of glycosidic bond breakage and water nucleophilic attack. CV2 is $\text{CN}_{\text{H}\text{Glu}187,\text{O}\text{Glu}187} - \text{CN}_{\text{O}4,\text{H}\text{Glu}187}$, which indicates proton transfer between the proton donor and the glycosidic oxygen atom. CN is defined as

$$\text{CN}_{ij} = \frac{1 - (d_{ij}/d^0)^p}{1 - (d_{ij}/d^0)^{p+q}}$$

where d_{ij} is the internuclear distance between atoms i and j , d^0 is the threshold distance for binding, and p and q are exponents that determine the steepness of CN_{ij} decay with respect to d_{ij} . CN values range from 0 (no bond) to 1 (a bond). In this case, $d^0 = 4.35$ au, $p = 12$, and $q = 3$ were chosen for CV1, and $d^0 = 2.44$ au, $p = 14$, and $q = 6$ were chosen for CV2. The fictitious masses of CV1 and CV2, required to implement the metadynamics technique in the Car–Parrinello MD scheme,^{22–24} were 15 and 5 amu, respectively, and the force constants of CV1 and CV2 were 1.5 and 1 au, respectively. Gaussian hills, 0.05 Å wide and 1.25 kcal mol⁻¹ high, were added to the potential well every 400 MD steps. The heights of these were small enough to ensure that the calculated free-energy surface is accurate.

Because of the loose nature of the XynB3 active site and the weak interaction between the aglycon product and the enzyme, the product xylosyl ring in subsite +1 showed a strong tendency to leave the binding pocket (this probably happens in Nature, as well, to clear the active site for a subsequent reaction). Nevertheless, in a metadynamics simulation, it is recommended that both the forward and backward reactions be observed before stopping the simulation to ensure an accurate free energy surface in both reactant and product sides. The tendency of the aglycon product to escape the active site prevented the backward reaction from occurring, even with the use of wall constraints. The absence of a backward reaction may lower the quality of the product side of the free energy surface (FES). In addition, the backward reaction usually lowers the barrier (~ 1 kcal/mol based on experience with other metadynamics simulations on GH enzymes)^{11,12} as the system explores the TS region again on its way to the reactant side.

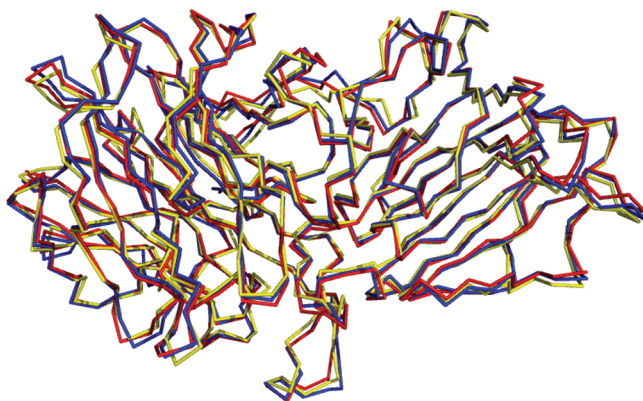


Figure 4. Superimposition of the XynB3 X-ray crystal structure (yellow) with the final structures from classical MD simulation (blue) and from metadynamics simulation (red). The superimposition was done to verify the validity of simulating XynB3 as a monomer.

3. Results and Discussion

3.1. Classical Molecular Dynamics Simulation.

Classical MD was performed on a monomer abstracted from the tetramer observed on the XynB3 crystal structure. The xylobiose molecule remains bound to the active site during the classical calculation, just as in the crystal structure. However, the 2S_0 ring conformation was not well maintained during the classical simulation, and it instead goes to the 4C_1 chair form (which is the most stable in solution). It has been observed that force fields are sometimes unable to predict the correct ring conformation, and more accurate electronic calculations are required to do this.⁸ To verify that removal of the proteins present in the tetramer did not affect the structural features of the simulated monomer, we superimposed the crystal structure with the final MD simulation structure and the final metadynamics (see below) structure. The rmsd between the MD simulated XynB3 and the crystal structure is 0.878 Å. The rmsd between the crystal structure and the last frame of the metadynamics simulation is 0.890 Å (Figure 4).

3.2. QM/MM Metadynamics Simulation. A total of 51 ps of metadynamics was required to model the enzymatic hydrolysis of xylobiose inside the GH43 β -xylosidase active site and to construct the FES (Figure 5). The glycosidic bond cleavage, with the simultaneous formation of a covalent bond between the nucleophilic water molecule and the anomeric carbon atom ($C1'$), occurred after 7 ps of metadynamics simulation. The rest of the 51 ps was spent exploring the product well, which is much deeper and longer than the reactant well.

3.3. Free Energy Surface and GH43-Catalyzed Hydrolysis. The Gaussian hills added to induce the reaction were used to construct the FES (Figure 5). Here, the reactant, TS, and product states can be identified. The free energy barrier was ~ 24 kcal/mol. Although no experimental energy barrier value was found for this enzymatic reaction, the calculated barrier lies in the range of experimental values found for other GHs.²⁵ The reaction's free energy (i.e., the difference between reactant and product free energies) was estimated at 30 kcal/mol.

All the structures from the metadynamics trajectory that correspond to each of the two minima (reactant and product) and the TS were selected to compute an average of important distances (Table 1). Representative structures for the reactant, TS, and product states are shown in Figure 6.

The reaction starts with the xylobiose molecule bound to the enzyme's active site, with its glycon pyranosyl ring distorted away from the most stable 4C_1 chair form (see below). The

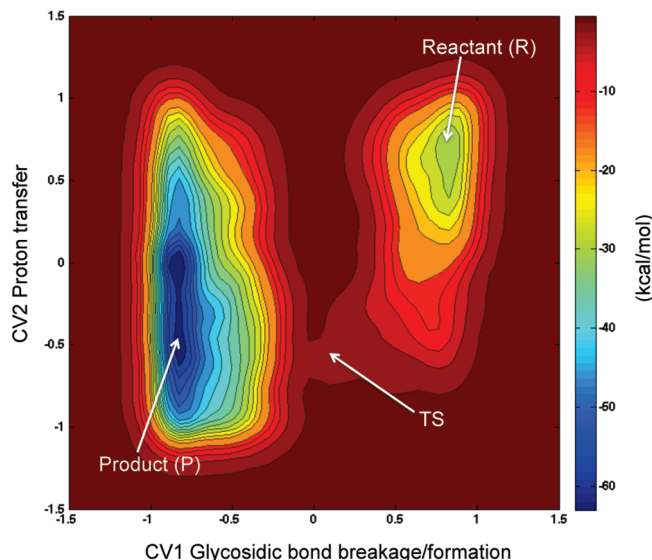


Figure 5. Free energy surface of β -xylobiose hydrolysis by GH43 β -xylosidase. Contours are separated by 3 kcal/mol.

TABLE 1: Average Bond Distances and Their Standard Deviations at Different Stages of the Reaction Pathway (Å)

| bond | reactants | TS | products |
|-------------------------|-----------------|-----------------|-----------------|
| $C1'-O4$ | 1.49 ± 0.04 | 2.62 ± 0.11 | 4.05 ± 0.32 |
| $C1'-O_{Wat}$ | 4.12 ± 0.19 | 2.75 ± 0.06 | 1.45 ± 0.04 |
| $O_{Glu187}-H_{Glu187}$ | 1.03 ± 0.03 | 1.56 ± 0.09 | 1.37 ± 0.13 |
| $H_{Glu187}-O4$ | 1.56 ± 0.06 | 1.03 ± 0.02 | 1.11 ± 0.07 |
| $O_{Asp15}-H_{Wat1}$ | 1.99 ± 0.27 | 1.83 ± 0.13 | 1.00 ± 0.03 |
| $N_{His249}-H_{Wat2}$ | 1.87 ± 0.12 | 2.00 ± 0.02 | 1.99 ± 0.21 |
| $H_{Arg288}-O_{Wat}$ | 3.07 ± 0.32 | 2.59 ± 0.06 | 2.72 ± 0.31 |
| $O_{Wat}-H_{Wat1}$ | 0.99 ± 0.03 | 0.99 ± 0.02 | 2.13 ± 0.39 |
| $C1'-O5'$ | 1.40 ± 0.02 | 1.28 ± 0.00 | 1.42 ± 0.03 |

scissile glycosidic bond is 1.49 Å long at the reactant state. The nucleophilic water molecule is held in place, 4.12 Å underneath the anomeric carbon atom, by forming a 1.99-Å-long hydrogen bond with the proton acceptor (Asp15) and a 1.87-Å-long hydrogen bond with His249. A weaker 3.07 Å hydrogen bond with active-site amino acid residue Arg288 also orients the water molecule for catalysis. The proton donor (Glu187) forms a 1.56-Å-long hydrogen bond with the scissile glycosidic oxygen atom (Figure 6).

When the TS is reached, the glycosidic bond elongates substantially to 2.62 Å, and the nucleophilic water molecule approaches within 2.75 Å of the anomeric carbon atom. The proton acceptor (Asp15) tightens its hydrogen bond with the nucleophilic water molecule from 1.99 Å at the reactant state to 1.83 Å at the TS. The $C1'$ atom becomes sp²-hybridized, forming a partial double bond with the ring oxygen atom ($O5'$), as evidenced by a shortening of the $C1'-O5'$ bond from 1.40 Å at the reactant state to 1.28 Å at the TS. This is consistent with a TS with significant oxacarbenium ion character.

The TS then collapses to the products, where the glycosidic oxygen atom ($O4$) is now 4.05 Å away from the $C1'$ atom, and the nucleophilic water molecule forms a covalent bond of 1.45 Å with the anomeric carbon atom, transferring the extra proton to the proton acceptor (Asp15) to finish the reaction. The $C1'$ atom recovers sp³ hybridization with a $C1'-O5'$ distance of 1.42 Å.

The lateral aspartate Asp128 forms a bidentate interaction with the $C2'-OH$ and $C3'-OH$ hydroxyl groups throughout the reaction. An analogous interaction was observed experimentally and computationally in a GH8 endoglucanase.^{11,26} The

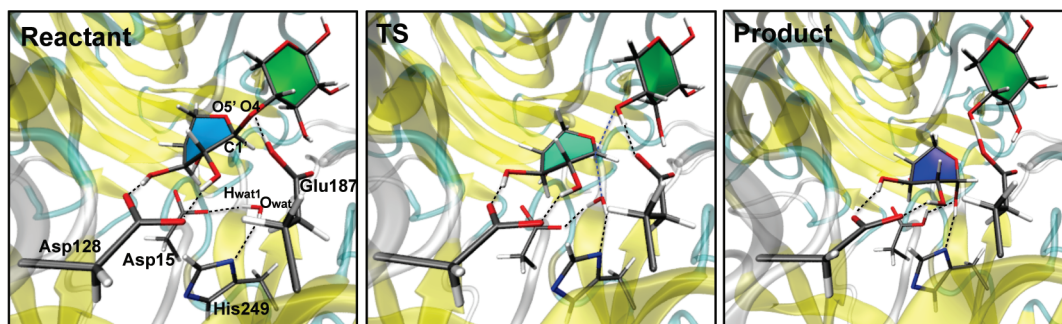


Figure 6. Structures for important states along the reaction pathway. Left panel, reactant; center panel, TS; right panel, product. The enzyme is shown in the background with β -sheets in yellow and loops in cyan, respectively.

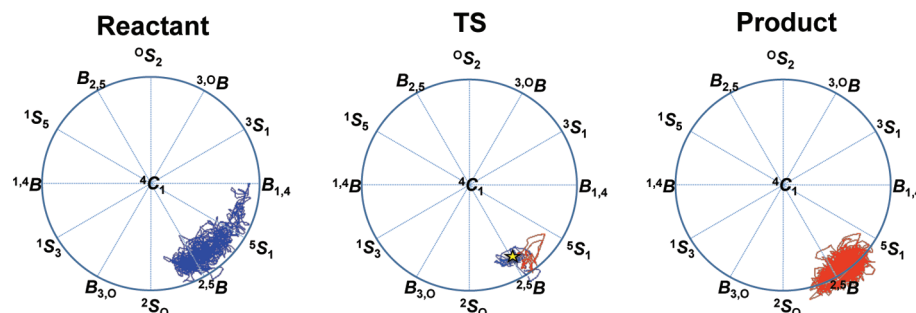


Figure 7. Conformational itinerary of the glycan xylosyl ring along the metadynamics simulation. The conformations visited before the TS are shown in blue on the left diagram. The conformations visited after the TS are shown in red on the right diagram. In the middle diagram, the average TS conformation is shown with a yellow star. The blue and red lines in the middle diagram represent the conformations visited immediately before and after the reaction, respectively (see text).

interaction of a negatively charged amino acid residue with the hydroxyl groups, especially the C2'-OH group, is likely to help relieve the electron deficiency of the TS, thereby providing a stabilizing effect.

3.4. Conformational Itinerary of GH43 β -Xylosidase. As mentioned above, the crystal structures of GH43 β -xylosidase, one a proton donor mutant (E187G) and the other missing an active-site lateral aspartate (D128G), have bound ligands with distorted glycan conformations. No wild-type crystal structure has a bound substrate or inhibitor. Because both crystal structures are tetramers, they hold eight xylobiose molecules, four with $^2\text{S}_0$ -like conformations, three with $^4\text{C}_1$ forms, and one with an ^0E . Because $^2\text{S}_0$ was the most populated form, we started the QM/MM simulation of the wild-type XynB3 with this glycan ring conformation. We tracked the glycan xylosyl ring conformation along the metadynamics simulation to verify that $^2\text{S}_0$ was a stable reactant conformation and to gain insight into the conformational itinerary of GH43 β -xylosidase along the reaction pathway. Although some conformers at the reactant stage fall between $^2\text{S}_0$ and $^{2.5}\text{B}$, none falls right on $^2\text{S}_0$. This indicates that the active-site mutations slightly affect the ring conformation at the reactant stage, as observed in the crystal structures. The conformations visited during the reaction were mapped onto a two-dimensional projection of the Cremer-Pople sphere²⁷ viewed from the north pole (Figure 7).

Reactant conformations span a significant range, from near $^2\text{S}_0$ all the way to $\text{B}_{1,4}$. This suggests, as do the mutated crystal structures with different ligand conformations, that the active site does not hold the glycan ring very tightly. The average xylosyl ring conformation at the TS has a structure very close to $^{2.5}\text{B}$, represented in the middle sphere by a yellow star. The $^{2.5}\text{B}$ conformation of the TS positions the C1', C2', C5', and O5' ring atoms in a plane. This planarity, intrinsic to six-member ring sugar oxocarbenium ions, is due to the formation of a partial double bond between the C1' and O5' atoms as the xylobiose

molecule proceeds to the TS. This was observed in the metadynamics reaction as a decrease in the C1'-O5' bond length at the TS (1.28 Å) compared to reactant or product states (1.40 and 1.42 Å, respectively) (Table 1). After the TS, a smaller region of the Cremer-Pople sphere, mainly between the $^{2.5}\text{B}$ and $^5\text{S}_1$ conformations, was populated.

Interestingly, this conformational itinerary is similar to the one previously found in an unrelated GH8 endoglucanase,¹¹ another inverting enzyme that catalyzes hydrolysis through a $^2\text{S}_0 \rightarrow {^{2.5}\text{B}} \rightarrow {^5\text{S}_1}$ type itinerary. However, in that case, the reactant glycan glucopyranosyl ring was found between a $^2\text{S}_0$ and a $^{2.5}\text{B}$ conformation before reaching the TS, whereas in this case, the glycan xylopyranosyl ring immediately moved to $^{2.5}\text{B}$, $^5\text{S}_1$, and $\text{B}_{1,4}$ conformations. Furthermore, a crystal structure from GH6 was also observed with a $^2\text{S}_0$ ring conformation in its binding pocket,²⁸ and it was later speculated that a nearby $^{2.5}\text{B}$ may be the GH6 TS conformation.¹⁰ This may be an example of convergent evolution, in which these enzymes arrived at a similar ring distortion strategy to perform hydrolysis and invert the configuration of the anomeric carbon of similar substrates, such as xylosyl and glucosyl oligomers.

To summarize, the GH43-catalyzed hydrolysis of xylobiose was modeled with first-principles Car-Parrinello QM/MM metadynamics. The FES of the reaction was constructed, allowing the identification of the important states along the reaction. Previously unknown structural information for the wild-type Michaelis complex, TS, and product was obtained with the simulation. The active site can accommodate a range of xylosyl ring conformations, especially at the Michaelis complex.

Acknowledgment. The authors thank the Iowa State University High Performance Computation System for making its facilities available to us. We also thank the National Research Initiative of the U.S. Department of Agriculture Cooperative

State Research, Education and Extension Service (Grant no. 2007-35504-18252) for its financial assistance.

References and Notes

- (1) Wolfenden, R.; Snider, M. J. *Acc. Chem. Res.* **2001**, *34*, 938–945.
- (2) Koshland, D. E. *Biol. Rev. Camb. Phil. Soc.* **1953**, *28*, 416–436.
- (3) Cantarel, B. L.; Coutinho, P. M.; Rancurel, C.; Bernard, T.; Lombard, V.; Henrissat, B. *Nucleic Acids Res.* **2009**, *37*, 233–238. www.cazy.org.
- (4) Brux, C.; Ben-David, A.; Shallom-Shezifi, D.; Leon, M.; Niefind, K.; Shoham, G.; Shoham, Y.; Schomburg, D. *J. Mol. Biol.* **2006**, *359*, 97–109.
- (5) Shallom, D.; Leon, M.; Bravman, T.; Ben-David, A.; Zaide, G.; Belakhov, V.; Shoham, G.; Schomburg, D.; Baasov, T.; Shoham, Y. *Biochemistry* **2005**, *44*, 387–397.
- (6) Simmott, M. L. *Chem. Rev.* **1990**, *90*, 1171–1202.
- (7) Davies, G. J.; Ducros, V. M.; Varrot, A.; Zechel, D. L. *Biochem. Soc. Trans.* **2003**, *31*, 523–527.
- (8) Biarnes, X.; Nieto, J.; Planas, A.; Rovira, C. *J. Biol. Chem.* **2006**, *281*, 1432–1441.
- (9) Biarnes, X.; Ardevol, A.; Planas, A.; Rovira, C.; Laio, A.; Parrinello, M. *J. Am. Chem. Soc.* **2007**, *129*, 10686–10693.
- (10) Vocadlo, D. J.; Davies, G. J. *Curr. Opin. Chem. Biol.* **2008**, *12*, 539–555.
- (11) Petersen, L.; Ardevol, A.; Rovira, C.; Reilly, P. J. *J. Phys. Chem. B* **2009**, *113*, 7331–7339.
- (12) Petersen, L.; Ardevol, A.; Rovira, C.; Reilly, P. J. *J. Am. Chem. Soc.* **2010**, *132*, 8291–8300.
- (13) Pearlman, D. A.; Case, D. A.; Caldwell, J.; Ross, W. S.; Cheatham, T. E.; DeBolt, S.; Ferguson, D.; Seibel, G.; Kollman, P. *Comput. Phys. Commun.* **1995**, *91*, 1–41.
- (14) Hornak, V.; Simmerling, C. *Proteins* **2003**, *51*, 577–590.
- (15) Kirschner, K. N.; Yongye, A. B.; Tschampel, S. M.; Gonzalez-Outeirino, J.; Daniels, C. R.; Foley, B. L.; Woods, R. J. *J. Comput. Chem.* **2008**, *29*, 622–655.
- (16) Jorgensen, W.; Chandrasekhar, J.; Madura, J.; Impey, R.; Klein, M. *J. Chem. Phys.* **1983**, *79*, 926–935.
- (17) Car, R.; Parrinello, M. *Phys. Rev. Lett.* **1985**, *55*, 2471–2474.
- (18) Laio, A.; VandeVondele, J.; Rothlisberger, U. *J. Chem. Phys.* **2002**, *116*, 6941–6947.
- (19) Troullier, N.; Martins, J. L. *Phys. Rev. B, Condens. Matter* **1991**, *43*, 1993–2006.
- (20) Perdew, J. P.; Burke, K.; Ernzerhof, M. *Phys. Rev. Lett.* **1996**, *77*, 3865–3868.
- (21) Ireta, J.; Neugebauer, J.; Scheffler, M. *J. Phys. Chem. A* **2004**, *108*, 5692–5698.
- (22) Laio, A.; Parrinello, M. *Proc. Natl. Acad. Sci. U.S.A.* **2002**, *99*, 12562–12566.
- (23) Iannuzzi, M.; Laio, A.; Parrinello, M. *Phys. Rev. Lett.* **2003**, *90*, 238302.
- (24) Ensing, B.; Laio, A.; Parrinello, M.; Klein, M. L. *J. Phys. Chem. B* **2005**, *109*, 6676–6687.
- (25) Yang, Y.; Hamaguchi, K. *J. Biochem.* **1980**, *88*, 829–836.
- (26) Guerin, D. M.; Lascombe, M. B.; Costabel, M.; Souchon, H.; Lamzin, V.; Beguin, P.; Alzari, P. M. *J. Mol. Biol.* **2002**, *316*, 1061–1069.
- (27) Cremer, D.; Pople, J. A. *J. Am. Chem. Soc.* **1975**, *97*, 1354–1358.
- (28) Zou, J.; Kleywegt, G. J.; Stahlberg, J.; Driguez, H.; Nerinckx, W.; ClaeysSENS, M.; Koivula, A.; Teeri, T. T.; Jones, T. A. *Structure* **1999**, *7*, 1035–1045.

JP107886E